On the role of the edge density profile for the L-H transition power threshold in ASDEX Upgrade

L.M. Shao[1,2], E. Wolfrum[1], F. Ryter[1], G. Birkenmeier[1,3], F.M. Laggner[4], E. Viezzer[1], R. Fischer[1], M. Willensdorfer[1], B. Kurzan[1], T. Lunt[1] and the ASDEX Upgrade Team

[1] Max-Planck-Institut für Plasmaphysik, Boltzmannstr. 2, 85748 Garching, Germany
[2] Institute of Plasma Physics, Chinese Academy of Sciences, Hefei 230031, People's Republic of China
[3] Physik-Department E28, Technische Universität München, 85748 Garching, Germany
[4] Institute of Applied Physics, TU Wien, Fusion@ÖAW, Wiedner Hauptstr. 8-10, 1040 Vienna, Austria

E-mail: shaolm@ipp.mpg.de

September 2015

Abstract. The L-H transition power threshold ($P_{\text{L-H}}$) in full tungsten (W) wall discharges is lower by 25% compared to those with graphite (C) mix tungsten walls in ASDEX Upgrade [Ryter F, *et al.* 2013 *Nucl. Fusion*]. The lower power threshold in the full tungsten wall discharges has been found to correlate with higher edge density as well as steeper edge density gradient. An estimate of the minimum in the neoclassical radial electric field well inside the separatrix yields a constant value for all analyzed L-H transitions at fixed toroidal magnetic field (B_{T}). The decrease of the threshold power is explained by the steeper edge density gradient in the discharges with full tungsten wall.

1. Introduction

The high confinement mode (H-mode), accessed generally above a certain heating power ($P_{\text{L-H}}$), is the baseline scenario for ITER discharges. The power threshold is an important issue, because at first ITER will be operated with heating power marginally above the L-H power threshold according to the latest and widely used ITPA threshold scaling for deuterium plasma [1]. On ASDEX Upgrade, the graphite and CFC (carbon fiber reinforced carbon) tiles were replaced stepwise by tungsten plasma facing components (PFCs) starting from 2003 and ending in 2007 [2]. Surfaces cleaning was executed as soon as the PFCs were fully covered by tungsten. A decrease of the power threshold of about 25% for the H-mode standard shots was found when the full tungsten coverage of PFCs was reached [3, 4]. Similar studies of the L-H transition were carried out with matched plasma current and toroidal magetic field pairs and plasma configurations in JET, where $P_{\text{L-H}}$ decreased $\sim$30% with JET beryllium/tungsten

wall (JET-ILW) compared to JET carbon wall (JET-C) at the plamsa density above the minimum plasma density [5]. Effect of effective charge (Z_{eff}) and its influence on turbulence stability [6] as well as plasma shape [5] were discussed as possible players. Moreover, the X-point position [7], the location of the strike point in the divertor [8] and the impact of gas puffs [9, 10] were found to influence $P_{\text{L-H}}$, which suggests that the edge density profile plays a role. In the present work we investigate the changes in the edge density profile as a possible explanation for the reduced $P_{\text{L-H}}$ in ASDEX Upgrade with the full tungsten wall.

In several devices zonal flows are observed to be driven by turbulence and subsequently quench turbulence in cycles just before the L-H transition [11, 12, 13], being an indication that sheared flows can suppress turbulence. At the same time, kinetic profiles become steeper. Neoclassical theory predicts that the edge radial electric field (E_r) is mainly driven by the main ion species [14, 15]. At the plasma edge, where the contribution of the perpendicular velocity component is small, E_r is mainly determined by the main ion pressure gradient. The steepening of the profiles due to additional heating or the interaction of zonal flows on turbulence can lead to an increase of the gradient of E_r and the associated $E \times B$ flow. The plasma stays in H-mode as soon as the flow shear driven by the main ion profiles are large enough to permanently reduce turbulent transport at the plasma edge and an edge transport barrier for particles and heat is formed just inside the separatrix (last closed flux surface). Therefore, the power threshold is determined by the main ion kinetic profiles with both the density and the temperature profiles and their gradients playing a crucial role [16, 17, 18].

In ASDEX Upgrade, the edge E_r is derived by applying the radial force balance equation to data of two active edge charge exchange recombination spectroscopy (CXRS) diagnostics [19, 20, 21] since 2011. Although there is no direct experimental evidence of the neoclassic nature of the measured E_r in L-mode, the neoclassic nature of E_r at the plasma edge has been confirmed by CXRS measurements in H-modes [22, 23, 24]. At ASDEX Upgrade it has been shown that, at fixed B_{T} and magnetic configuration, the minimum in the neoclassical radial electric field ($E_{r,\text{neo}}$) at the L-H transition is almost independent of density in the full tungsten wall [25]. Here, the authors neglected the effect of plasma parallel rotation, because the bulk parallel flow speed is small at the edge of L-mode plasmas and has a lower contribution to $E_{r,\text{neo}}$ than the main ion pressure gradient. A fairly constant value of the $E \times B$ flow across a range of toroidal magnetic field and line-averaged densities was also observed in both JET-ILW and JET-C [5]. These observations at ASDEX Upgrade and JET indicate that the $E \times B$ flow may be the parameter behind the L-H transition physics. Although, there are no direct measurements of E_r in this study, because the CXRS diagnostic was not available for most discharges in the dataset, the behavior of edge profiles and the possible impact on the E_r well are analyzed at the L-H transition. In an attempt to understand the decrease of $P_{\text{L-H}}$ after the transition from carbon wall to tungsten wall, in this paper we investigate the changes in the edge profiles and try to relate it to the L-H transition power threshold.

The paper is organized as follows. Section 2 describes the experimental setup and comparisons of edge parameters, as edge electron density, temperature, pressure and density gradient in different PFCs. The effect of divertor detachment and reflection coefficient of

wall on edge plasma density is revealed in section 3. A detailed description of evaluating the minimum of the neoclassical radial electric field at the plasma edge is presented in section 4. The discussion and conclusions are shown in the last section.

2. Experiments and comparison of edge parameters

ASDEX Upgrade is a medium size tokamak with major radius $R = 1.65$ m and minor radius $a = 0.5$ m. Since 1999 at ASDEX Upgrade, the so-called 'H-mode standard shot' run as the first plasma discharge of each operation day, is meant to yield a survey of long term evolution of the L-H transition and confinement properties [26]. It is run in the usual lower single null magnetic configuration with ion ∇B drift towards the active X-point. The L-H transition is induced by a power ramp of neutral beam injection (NBI) achieved by beam modulation with increasing duty-cycle. The 'H-mode standard shot' was originally run at $|B_{\mathrm{T}}| = 2.0$ T, but this had to be increased to $|B_{\mathrm{T}}| = 2.5$ T when the tungsten coverage of the vacuum vessel increased [4]. Therefore, the number of discharges run at $|B_{\mathrm{T}}| = 2.5$ T is limited which severely restricts the possibilities to compare between carbon wall and full tungsten wall [4].

Detailed edge density and temperature profiles are important to study the neoclassical E_r. The electron density (n_{e}) profiles are provided by lithium beam impact excitation spectroscopy (Li-IXS) utilizing a probabilistic data analysis method based on Bayesian probability theory (BPT) [27]. The 35 channels offer a spatial resolution of 5 mm and a temporal resolution better than 1 ms. The electron temperature (T_{e}) profiles in carbon wall discharges are given by electron cyclotron emission (ECE) applying forward modeling within the integrated data analysis (IDA) frame [28]. This analysis is able to quantitatively reproduce the measured electron radiation intensities for all frequencies in both optically thick and thin plasma regions. For the full tungsten wall discharges, T_{e} profiles mainly provided by combining core Thomson scattering (core TS) and edge Thomson scattering (edge TS) are used [29]. The ion temperature (T_{i}) profiles are acquired with two edge systems of CXRS with viewing chords in both toroidal [19] and poloidal [20] directions (only in full tungsten wall). Unfortunately, there are only 7 shots with edge T_{i} profiles available in the 'H-mode standard shot' dataset. The complete dataset at $|B_{\mathrm{T}}| = 2.5$ T consists of 11 carbon wall (69% W coating PFCs) discharges with core line-averaged densities of about 4.5×10^{19} m^{-3} (2 shots) and 5×10^{19} m^{-3} (9 shots), and 14 discharges with full tungsten PFCs with a core line-averaged density around 5×10^{19} m^{-3}. The plasma core line-averaged density as well as edge line-averaged density are measured by deuterium cyanide (DCN) interferometer with tangency radii $\rho_{\mathrm{pol}} \approx 0.10$ and $\rho_{\mathrm{pol}} \approx 0.87$, respectively [30]. ρ_{pol} is the normalized poloidal flux coordinate ($\rho_{\mathrm{pol}} = \sqrt{\frac{\Psi - \Psi_{\mathrm{axis}}}{\Psi_{\mathrm{sep}} - \Psi_{\mathrm{axis}}}}$).

The dataset varies in plasma shape and location of gas fuelling (from the main chamber or lower divertor region). By comparing various shapes in both PFCs as well as dedicated experiments in the full tungsten wall discharges, in which we used both main chamber and

divertor fuelling, we verified that these variations have no impact on $P_{\text{L-H}}$. The carbon concentration of ∼0.8% in the tungsten wall discharges is much less compared to the ones with carbon walls (∼1.5%) [3]. However, in the 2008 campaign with the full tungsten wall $P_{\text{L-H}}$ was reduced ∼ 25% without boronization where the carbon content is close to that in carbon wall discharges [4]. We also attempted to mimic the presence of carbon with nitrogen seeding in the full tungsten wall 'H-mode standard shot' discharges, and no increased $P_{\text{L-H}}$ was found [4].

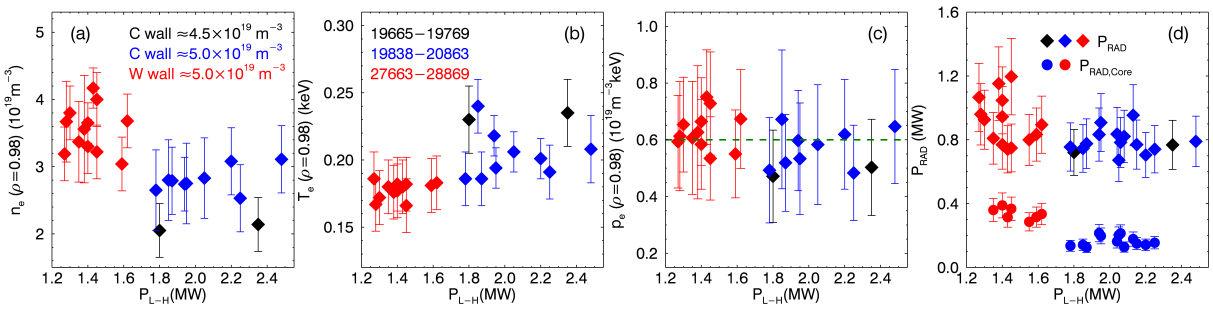

Figure 1: Edge (a) electron densities, (b) electron temperatures, (c) electron pressures at $\rho_{\text{pol}} = 0.98$ and (d) total (core and divertor) as well as core plasma radiated power versus power thresholds. The black and blue diamonds are from discharges in C wall with core line-averaged densities separately of 4.5 and 5×10^{19} m^{-3}, and the red diamonds represent the shots in full tungsten PFCs with a core line-averaged density of 5×10^{19} m^{-3}.

In figures 1(a)-(c) we compare the values of edge plasma parameters at $\rho_{\text{pol}} = 0.98$ in carbon and full tungsten walls just before the L-H transition by plotting these quantities versus $P_{\text{L-H}}$. These quantities are electron densities (taken in a time interval of 40 ms), temperatures (taken in a time interval of ∼ 60 ms) and pressures. The power threshold values are obtained from the loss power (P_{loss}) at the L-H transition,

$$P_{\text{loss}} = P_{\text{heat}} - dW/dt. \tag{1}$$

Here P_{heat} is the sum of Ohmic and auxiliary heating powers subtracting the loss and unabsorbed parts of injected powers, and W is the plasma stored energy. The plasma stored energy is calculated in the usual way from the magnetic equilibrium (W_{MHD}). From this value, the thermal plasma energy can be deduced by subtracting the NBI fast ion energy. The dW/dt term is the largest source of experimental uncertainties during a heating power ramp. Nevertheless, it is not significant compared to P_{heat} during the heating power ramps in our dataset. Figure 1 indicates that $P_{\text{L-H}}$ is clearly lower with the full tungsten wall than with the carbon wall. The errorbars of $P_{\text{L-H}}$ for the dataset are 10-20% of their own values. Higher electron densities and lower temperatures at $\rho_{\text{pol}} = 0.98$ are found in the discharges with full tungsten PFCs. The electron pressures seem comparable at $\rho_{\text{pol}} = 0.98$ in both PFCs. The total radiated power (P_{RAD}) of the plasma including the core and divertor regions is also close in both PFCs discharges as shown in figure 1(d). To increase the confidence of this trend, some 'H-mode standard shot' discharges in the same campaigns of our dataset with

Li-IXS unavailable are also shown in figure 1(d). However, the radiated power from the core plasma $P_{\mathrm{RAD,Core}}$ is a bit higher in the full tungsten wall discharges compared to the carbon walls. Both the total and core radiated powers are derived from the bolometric line-integrals of radiation [31]. It should be emphasized that, due to lower temperature and higher density, the collisionality in the full tungsten PFC discharges at $\rho_{\mathrm{pol}} = 0.98$ is different from that in discharges with the carbon wall at the same core line-averaged density of 5×10^{19} m^{-3} . The expression of the ion collisionality [32] is

$$\nu_{*\mathrm{i}} = 4.90 \times 10^{-18} \frac{qRn_{\mathrm{i}} \ln\Lambda_{\mathrm{ii}}}{T_{\mathrm{i}}^2 \epsilon^{3/2}}. \tag{2}$$

$$\ln\Lambda_{\mathrm{ii}} = 30 - \ln(\frac{\sqrt{n_{\mathrm{i}}}}{T_{\mathrm{i}}^{3/2}}). \tag{3}$$

Here, q is the safety factor and ϵ is the inverse aspect ratio. The ion collisionality here is the ion-ion collision frequency normalized to the bounce frequency. The collionality is much higher in the full tungsten PFC discharges ($\nu_{*\mathrm{i}} \in [3.46, 4.64]$) than that in the carbon walls ($\nu_{*\mathrm{i}} \in [1.30, 2.11]$) using $n_{\mathrm{i}} = n_{\mathrm{e}}$ and $T_{\mathrm{i}} = T_{\mathrm{e}}$ at $\rho_{\mathrm{pol}} = 0.98$ [32].

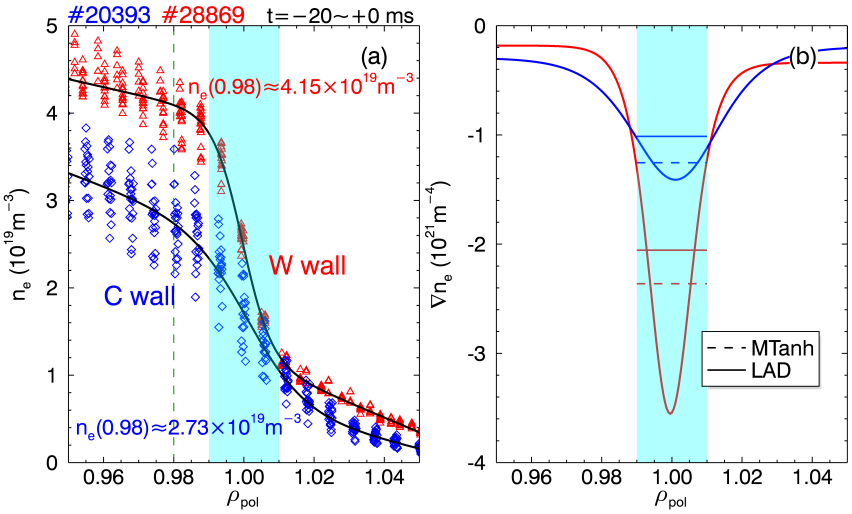

Figure 2: (a) Edge density profiles comparison in a time interval of 20 ms before till the L-H transition of NBI heated plasmas. #20393 (blue open diamonds, C wall) and #28869 (red open triangles, W wall) share the same core line-averaged density. The black curves are density profiles fitted with a modified hyperbolic tangent (MTanh) function. (b) Edge density gradient profiles comparison of the two discharges. The edge density gradient profiles are achieved by fitting the edge density profiles with MTanh. The horizontal solid lines are averaged density gradients applying MTanh, while the horizontal dashed lines are edge density gradients utilizing the least absolute deviation function in the cyan region of (a).

Figure 2(a) shows a comparison of typical edge electron density profiles with the same core line-averaged density for two H-mode standard discharges within different plasma facing materials. The time slices for the edge density profile data are taken in a time interval of 20

ms just before the L-H transition. Although the selected time slices are still in L-mode, a clear pedestal-like shape of the profiles is visible in the density (not in the temperature). The discharge #28869, run with full metal wall, exhibits a higher edge density at $\rho_{\rm pol} = 0.98$ (the green vertical dashed line in figure 2(a)) and a steeper edge density gradient $\nabla n_{\rm e}$ compared to #20393 with carbon PFCs. The black curves are edge density profiles fitted with a modified hyperbolic tangent (MTanh) function [33]. The edge density gradient profiles derived from the MTanh fit are shown in figure 2(b). The edge density gradient values used in the following are achieved from averaging $\nabla n_{\rm e}$ from the MTanh fit in the steep edge region, typically $\rho_{\rm pol}$ =0.99-1.01 (cyan regions in figure 2) or fitting the density profiles in the same region utilizing the least absolute deviation (LAD) method [34]. These values are separately shown in figure 2(b) with horizontal dashed lines and solid lines. The values of $\nabla n_{\rm e}$ calculated with the two different methods lie within their respective uncertainties.

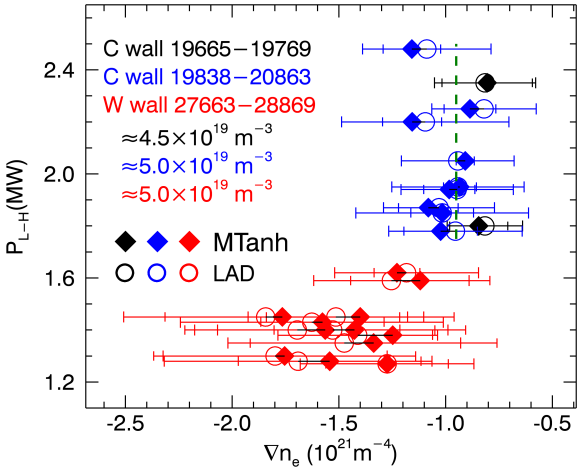

Figure 3: Power threshold versus edge density gradient. The edge density gradients are fitted by applying the MTanh function (filled diamonds) and the LAD function (open circles). The black and blue symbols are the discharges in C wall with core line-averaged densities of 4.5 and 5×10^{19} m^{-3}, while the red symbols are the shots in full W PFCs with a core line-averaged density of 5×10^{19} m^{-3}.

Figure 3 shows $P_{\rm L\text{-}H}$ versus the edge density gradients taken in a time interval of about 40 ms just before the L-H transition for our dataset. The black and blue symbols are discharges in carbon wall with core line-averaged densities of 4.5×10^{19} m^{-3} and 5×10^{19} m^{-3}, respectively. The red symbols are shots in full tungsten device with a core line-averaged density of 5×10^{19} m^{-3}. The edge density gradients are evaluated by fitting the edge density profiles applying the MTanh function (filled diamonds) and the LAD function (open circles). The errorbars in $\nabla n_{\rm e}$ applying the MTanh function (same color with the symbols) or the LAD function (black) are the standard deviations of the fits. The values of the edge density gradients calculated by these two methods are consistent. With values of about -1.5×10^{21} m^{-4} , steeper edge density gradients are found in the full tungsten wall discharges

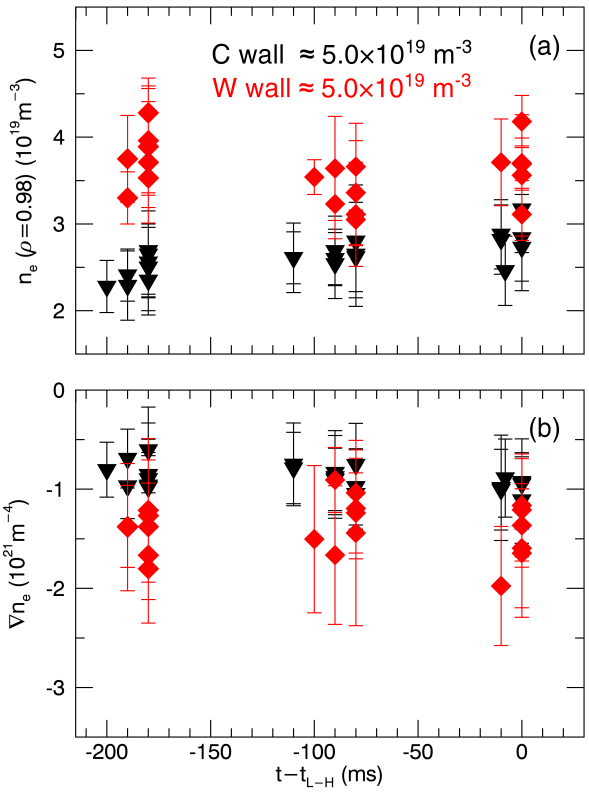

Figure 4: Time dependence of (a) the edge densities at $\rho_{\rm pol} = 0.98$ and (b) the edge density gradients ~ 200 ms before, ~ 100 ms before and just before the L-H transition for the dataset. The black triangles represent the shots in C wall and red diamonds stand for the discharges in full W wall. In both cases, the core line-averaged density is 5×10^{19} m^{-3}.

corresponding to the lower $P_{\rm L\text{-}H}$. In the carbon wall discharges, the edge density gradients are flatter, with values around -0.95×10^{21} m^{-4}, as expected from figure 1(a).

To investigate the role of the edge density profile for the L-H transition power threshold, besides the edge density at $\rho_{\rm pol} = 0.98$ and edge density gradient, their temporal evolution has been analyzed. Figure 4 shows the edge densities at $\rho_{\rm pol} = 0.98$ and edge density gradients averaged over time intervals of 20 ms taken at ~ 200 ms, ~ 100 ms and just before the L-H transition. All discharges here with both carbon (black triangles) and full tungsten (red diamonds) walls have the same core line-averaged density of 5×10^{19} m^{-3} just before the L-H transition. The edge density at $\rho_{\rm pol} = 0.98$ and the edge density gradient in panels (a) and (b) are systematically higher and steeper in the discharges with the full tungsten PFCs.

3. Causes for steeper edge plasma density profile

The reason for the steeper electron density gradients in full tungsten wall discharges was not immediately obvious. The position of gas fuelling (mid-plane or divertor) was ruled out as cause in dedicated discharges: the shape of the density profile could not be influenced by

changing the fuelling position. When comparing the evolution of discharges up to the L-H transition, we found that longer lasting fluctuating detachment states [35] occurred in the discharges with full tungsten wall. In the following the influence of the different detachment states on the edge density gradient is shown. First, we characterize the different detachment states with an example. For details the reader is referred to reference [35].

Figure 5 shows the temporal evolution of some important plasma quantities of a representative full tungsten wall discharge #27962 and a carbon wall discharge #20409 in the dataset before the L-H transition. The plasma is heated by NBI blips starting from 1.392 s for the tungsten wall discharge and 1.129 s for the carbon wall discharge. In panels (a), the plasma current, Ohmic and NBI heating powers, total plasma radiated power as well as the loss power are shown. The Ohmic power is evaluated by the product of the plasma loop voltage and plasma current, i.e. $P_{\mathrm{OH}} = U_{\mathrm{loop}} I_{\mathrm{p}}$. Here, U_{loop} is corrected for flux changes between the separatrix and measurement loop. Since only one NBI beam was turned on, the total NBI heating power expression can be written as $P_{\mathrm{NBI}} = U_{\mathrm{ex}} I_{\mathrm{ex}} T(U_{\mathrm{ex}})$. Where, U_{ex} is the extraction voltage, I_{ex} is the extracted beam current and T is the transmission of the beam line. The transmission depends on the extraction voltage and the beam quality, i.e. the divergence, and hence on the perveance and is measured by calorimetry. Then the total heating power P_{heat} in equation 1 can be written as $P_{\mathrm{heat}} = P_{\mathrm{OH}} + P_{\mathrm{NBI}} - P_{\mathrm{NBI,Loss}}$. Here, $P_{\mathrm{NBI,Loss}}$ is the loss part of the NBI injected power, including shine through, ripple loss, scrape-off layer (SOL) loss, charge exchange loss and prompt orbit loss, which are not absorbed by the plasma. The plasmas separately enter the H-mode at 1.564 s and 1.472 s indicated by a significant drop of the D_α signal measured from lower inner divertor region (see panels (b)) and a sharp increase of the plasma core and edge line-averaged densities (see panels (c)). The divertor temperature T_{div} evaluated from the lower inner divertor shunt current [36] is shown on the left-hand side of panel (b). The divertor shunt current is only available in the full tungsten wall discharges. The gas fuelling rate shown in panels (c) is controlled by the plasma density feed-back system.

The notation of the degree of detachment (DOD) shown in panels (d) and (e) is used to identify the detachment of the inner and outer divertor. The degree of detachment is defined as the ratio of the calculated to measured ion heat flux to the target [35]. Thus when DOD>1, the energy and pressure loss along a field line starts, hence divertor detachment begins. Since the strike point of the inner target of #20409 swept during the discharge, only a short phase with a stable strike point is shown on the right-hand side of panel (d). Please note that the increase of DOD before the L-H transition on the right-hand side of panel (e) is not caused by the detachment of the outer divertor but by a slow sweep of the strike point. Before the plasma enters the H-mode, a divertor detachment process over 600 ms is observed in #27962. The divertor detachment process can be divided into the onset detachment state (OS, 0.952-1.032 s, see panels (d) and (e) on the left-hand side), fluctuating detachment state (FS1, 1.032-1.270 s and FS2, 1.460-1.564 s) and complete detachment state (CDS, 1.270-1.460 s) [35]. The three states can be observed in the fast diode bolometers of the absolute power measurement in the Absolute eXtreme Ultra Violet

(AXUV) diagnostic, divertor temperature evaluated from divertor shunt current and even D_α signal and (outer divertor) Mirnov coil measurements. Panels (d) and (e) on the left-hand side are the temporal-frequency spectra of AXUV integrated signals located at the low- and high-field sides of the X-point of #27962, respectively. The fluctuating detachment state is a kind of radiative fluctuations in a low kHz-range appearing in the inner (outer) scrape-off layer close to the X-point.

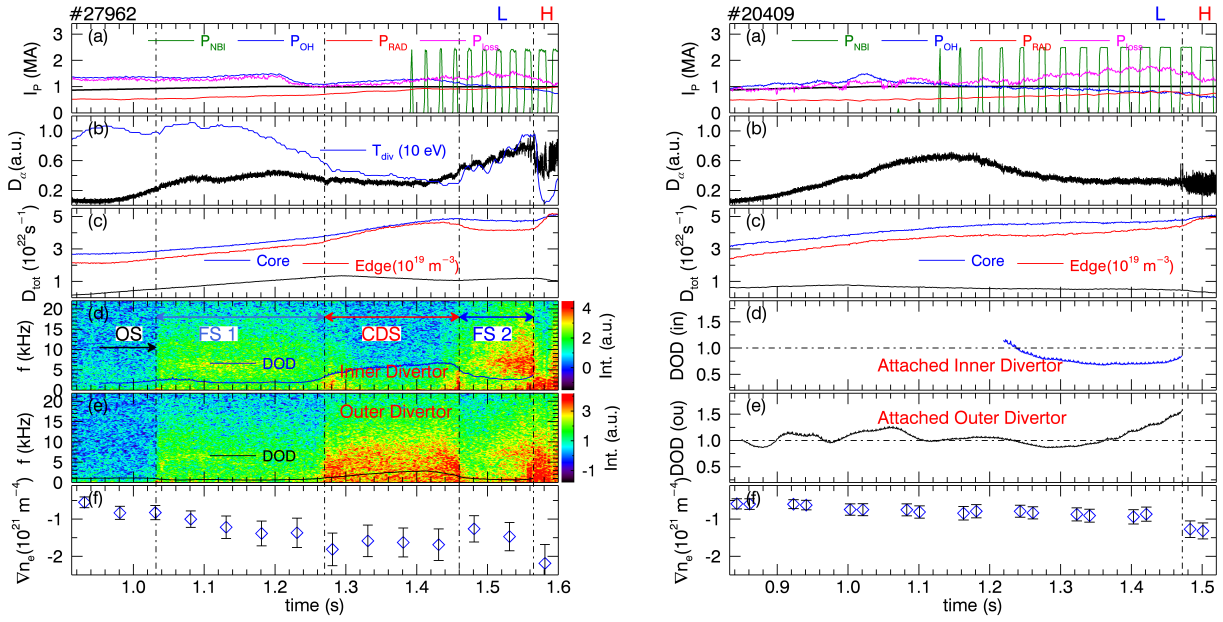

(a) #27962 Detachment

(b) #20409 Attachment

Figure 5: Left: W wall discharge #27962 (0.913-1.600 s), Right: C wall discharge #20409 (0.833-1.520 s). The time trace of (a) plasma current, NBI and Ohmic heating powers, total plasma radiated power as well as the loss power, (b) lower inner divertor D_α signal and divertor temperature $T_{\rm div}$ (only #27962), (c) gas fuelling rate, core and edge line-averaged densities, (d) inner and (e) outer divertor temporal-frequency spectrum of AXUV signals (only #27962) and degree of detachment (DOD) and (f) edge density gradient before the L-H transition. The plasmas of #27962 and #20409 enter the H-mode at 1.564 and 1.472 s, respectively.

When the plasma of #27962 enters the fluctuating divertor detachment phase at 1.032 s, the divertor temperature $T_{\rm div}$ decreases as shown in panel (b) on the left-hand side. In the meantime, the plasma core and edge line-averaged densities increase continuously. As soon as the plasma enters the complete divertor detachment state at 1.270 s, the plasma line-averaged density at the edge increases more strongly and the divertor temperature decreases monotonously. While at 1.460 s, the complete divertor detachment phase is mitigated and returns to the fluctuating divertor detachment state, both plasma core and edge line-averaged densities and divertor temperature go reversely. However, the divertor is always attached in

the carbon discharge #20409. On the right-hand side of panel (c) the time trace of the core and edge line-averaged densities of a carbon wall discharge #20409 are presented (see blue and red dotted lines). #20409 and #27962 have the same core line-averaged density just before the L-H transition. The gap between the core and edge line-averaged densities stays the same from far before to the L-H transition in the carbon wall discharge. While in the full tungsten wall discharge the core and edge line-averaged densities get closer and closer when the plasma enters the fluctuating detachment state and complete detachment state. Please note here, since the plasma magnetic shape is modified a bit in the full tungsten wall H-mode standard discharges from that of carbon wall discharges, the chord of edge line-averaged density is not exactly the same in the different PFCs discharges. Comparing the left- and right-hand side of panels (f), both the core line-averaged density and edge density gradient at ∼0.93 s in #27962 are close to those at ∼0.85 s in #20409. As soon as the plasma with the full tungsten wall enters the OS, ∇n_e becomes much steeper, and further steeper in FS1, and steepest in CDS. When CDS is mitigated, ∇n_e flattens although the gas fuelling rate varies only a little. Nevertheless, ∇n_e increases again steeper monotonously in #20409 concomitant with the core line-averaged density. ∇n_e in #27962 is steeper than in the carbon wall discharge #20409 since the divertor is detached.

Comparing discharges in different PFCs we find: In carbon PFCs discharges, only a short phase (∼ 40 ms) in the fluctuating divertor detachment state, starting at about 150 ms before the L-H transition, is visible. The phase disappears before (> 30 ms) the plasmas enter the H-mode. In the full tungsten wall discharges, however, the fluctuating state starts much earlier, i.e. already in the ohmically heated phase (∼ 400 ms before the NBI turns on). The fluctuating state lasts longer and it is mostly followed by a transition to the complete detachment state. The total period of fluctuating and complete divertor detachment is over 550 ms for most full tungsten wall discharges investigated in this work.

The edge density profiles measured by Li-IXS during a time window of 20 ms in the different divertor detachment phases of #27962 are shown in figure 6(a). The edge density profile becomes steeper as the divertor state transfers from attachment state (AS) to detachment states. These are revealed in figure 6(a), where the edge density top and edge density gradient of #27962 become higher and higher as well as steeper and steeper from AS (0.915-0.935 s) to OS (0.970-0.990 s) and to FS1 (1.120-1.140 s) till CDS (1.370-1.390 s). The edge density top drops down, when the complete divertor detachment state (red density profile) is mitigated and returns to fluctuating detachment state (FS2, 1.520-1.540 s). Unlike the full tungsten wall discharges, there is only a very short fluctuating detachment state in the carbon wall discharges. The edge density top and edge density gradient of a typical carbon wall discharge #20409 increase monotonously before the L-H transition as shown in figure 6(b). The same black, cyan, red and blue density profiles in figure 6(a) and (b) correspond to a similar core line-averaged density in different PFCs discharges. Comparing these density profiles, systematically steeper edge density profiles are found in full tungsten wall discharges already when the plasma enters the divertor detachment state. In full tungsten wall discharges, the density gradient at the steep density region becomes much steeper when

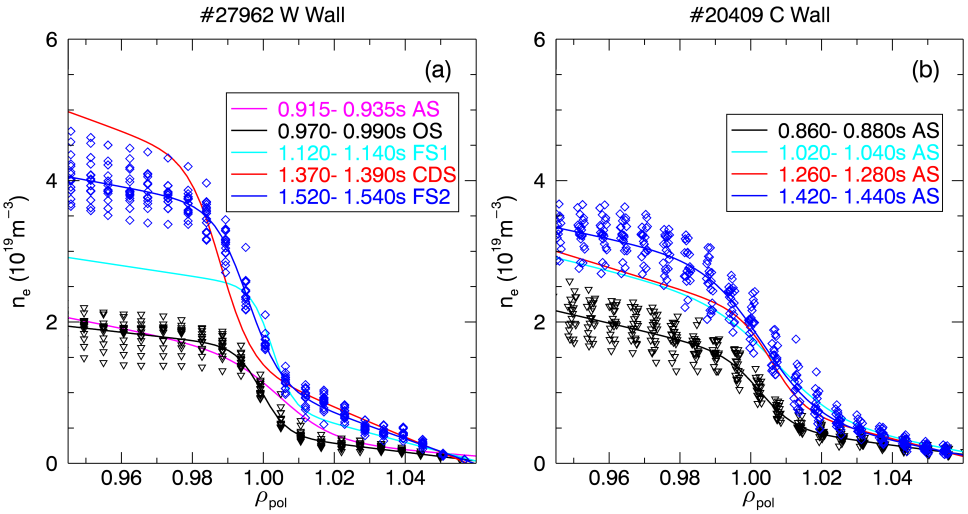

Figure 6: Edge electron density profiles versus ρ_{pol}. (a) Edge density profiles of #27962 in five time slices with a time window of 20 ms: 0.915-0.935 s (attachment state, AS), 0.970-0.990 s (OS), 1.120-1.140 s (FS1), 1.370-1.390 s (CDS) and 1.520-1.540 s (FS2). (b) Edge density profiles of #20409 in five time slices: 0.860-0.880 s, 1.020-1.040 s, 1.260-1.280 s and 1.420-1.440 s, when plasma all stay attachment state. The L-H transition time of #27962 and #20409 are 1.564 s and 1.472 s, respectively. Only the edge density profiles from Li-IXS in the black and blue time slices are shown here.

the divertor enters the detached state. That means, when two plasmas have the same core line-averaged density, the detached plasma has a steeper edge density gradient.

Not only plasmas in a phase with detached divertor show steeper edge density profiles in the full tungsten wall discharges. An experiment of two attached Ohmic plasmas with same plasma current and similar impurity concentration were operated in the carbon (#21305, 1.945-2.000 s) and full tungsten (#22060, 1.945-2.000 s) walls [37]. The steeper edge density profile is also found in the full tungsten wall case in these attached plasmas. One reason could be the reflection coefficient of deuterium, which is up to two times higher on tungsten than on carbon [38]. This higher reflection coefficient could lead to a higher neutral particle flux inside the separatrix, and thus provide an additional particle source.

With the aim of testing this hypothesis, simulations with the EMC3-Eirene code package [39] were carried out on the same grid as that used in reference [40] for 'case B'. This grid was created for the ASDEX Upgrade equilibrium of the full tungsten wall discharge #29887 at 4.430 s and extended radially until $\rho_{\mathrm{pol}} = 1.15$, i.e. beyond the main chamber plasma facing components (MC PFCs) located at $\rho_{\mathrm{pol}} = 1.038$ (inner heat shield) and $\rho_{\mathrm{pol}} = 1.05$ (ICRH limiters) that were included in the simulation. In contrast to the simulation of the 'case B' (and in contrast to the experiment) we assumed a much lower outboard midplane density $n_{\mathrm{e,OMP}} = 6 \times 10^{18}$ m^{-3} and a slightly higher input power $P_{\mathrm{in}} = 800$ kW (equally distributed between the ions and the electrons) here. In addition

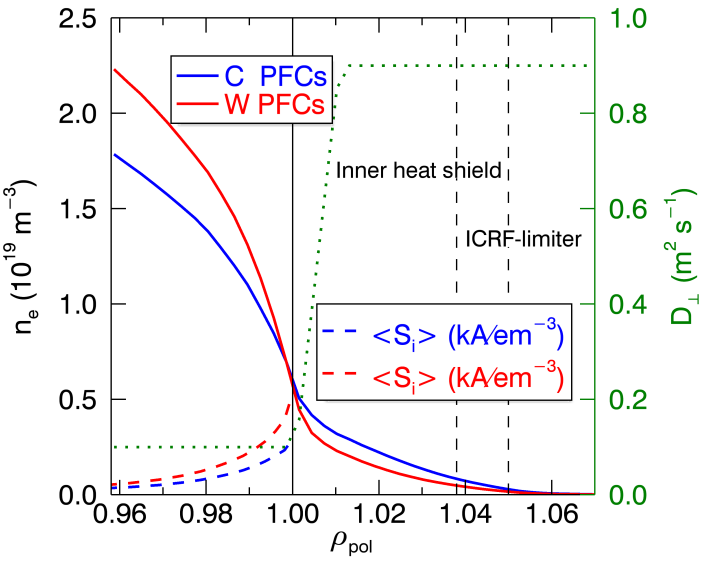

Figure 7: Simulation result of the effect of recycling coefficients of C and W PFCs on edge density profiles. Blue and red curves represent the edge density profile in C and W walls. The blue and red dashed curves are the ionization source profiles averaged over the flux surface in C and W walls. The green dotted line is the particle cross-field diffusion coefficient $D_\perp$.

to that we used the transport coefficients of 'case A' in reference [40], where the diffusive transport coefficients change from $D_\perp = 0.1$ m^{2}s^{-1} in the core to $D_\perp = 0.9$ m^{2}s^{-1} in the SOL (see green dotted curve in figure 7), with the heat cross-field diffusion coefficient $\chi_\perp = 3D_\perp$. Figure 7 shows the (local) density profiles at the outer midplane for the cases with carbon and with tungsten PFCs. The ionization source profiles averaged over the flux surface at the plasma edge are also shown in figure 7 (see blue and red dashed curves). It is found that the edge density profile is indeed steeper for the case with tungsten PFCs, which is explained by an enhanced ionization source in the confinement region. If this is a direct effect of the enhanced reflection energy of the neutrals from the wall, or if charge exchange processes in the SOL (where T_i is found to be higher in the tungsten wall case) play an important role and if the MC PFCs or the divertor PFCs are responsible for the effect will be investigated in the near future.

The above analysis of the divertor detachment and higher reflection coefficient of deuterium on tungsten give likely causes for the different temporal evolution of the edge density profiles in different PFCs discharges. However, a study of the decreased impurity concentration affecting the edge density profile in full tungsten wall discharges is missing. Nowadays, we only can test the impact of impurity concentration on edge density profile in the tungsten wall discharges with the attached divertor. Nevertheless, a higher impurity concentration, like nitrogen seeding, can easily drive the divertor into detachment in L-mode plasmas. The divertor detachment prevents us from investigating the impact of impurity concentration on edge density profiles. In figure 4, we have a clear indication that the

electron density profile systematically exhibits a steeper edge density gradient in the analyzed full tungsten wall discharges. The steeper edge density gradient, most probably caused by the divertor detachment as well as higher recycling coefficient with more energetic reflected particles of the full metal wall, seems to contribute to the lower $P_{\text{L-H}}$ values as discussed in the following.

4. Neoclassical radial electric field

As mentioned above, for fixed B_{T} and magnetic configuration, the L-H transition occurs at a given value of the minimum of the $E_{r,\text{neo}}$ well [25]. In the following, we investigate whether the minimum in $E_{r,\text{neo}}$ just before the L-H transition is the same with the carbon and full tungsten walls in our dataset. The neoclassical calculation of E_r is composed of the diamagnetic term $E_{r,\text{dia}}$, a term proportional to $\nabla T_{\text{i}}/e$ (e = electric charge) with a collisionality dependent factor α and a term proportional to the plasma mean parallel main ion velocity $\left\langle V_{\text{i}\parallel}\right\rangle$ [14]:

$$E_{r,\text{neo}} = E_{r,\text{dia}} - \alpha\frac{\nabla T_{\text{i}}}{e} + \frac{B}{B_{\text{t}}}B_\theta\left\langle V_{\text{i}\parallel}\right\rangle. \tag{4}$$

$$E_{r,\text{dia}} = \frac{\nabla P_{\text{i}}}{n_{\text{i}}e} = \frac{\nabla n_{\text{e}}}{n_{\text{e}}}\frac{T_{\text{i}}}{e} + \frac{\nabla T_{\text{i}}}{e}. \tag{5}$$

Here, the toroidal field B_{t} and poloidal magnetic field B_θ are determined by the equilibrium code CLISTE [41]. B is the total magnetic field and $B = \sqrt{{B_{\text{t}}}^2 + B_\theta^2}$. $B_{\text{t}} \approx 1.93$ T and $B_\theta \approx 0.34$ T at the low-field side plasma edge of our dataset. The main ion pressure is $P_{\text{i}} = n_{\text{i}}T_{\text{i}}$ and we assume $n_{\text{i}} = n_{\text{e}}$. Now, we estimate the last term in equation (4) as $\frac{B}{B_{\text{t}}}B_\theta\left\langle V_{\text{i}\parallel}\right\rangle \approx 0.35\left\langle V_{\text{i}\parallel}\right\rangle$ at the plasma edge in ASDEX Upgrade. Combining equations (4) and (5), the neoclassical E_r equation can be written as

$$E_{r,\text{neo}} = \frac{\nabla n_{\text{e}}}{n_{\text{e}}}\frac{T_{\text{i}}}{e} + (1-\alpha)\frac{\nabla T_{\text{i}}}{e} + \frac{B}{B_{\text{t}}}B_\theta\left\langle V_{\text{i}\parallel}\right\rangle \tag{6}$$

$$= \frac{\nabla n_{\text{e}}}{n_{\text{e}}}\frac{T_{\text{i}}}{e} + (1-\alpha)\frac{\nabla T_{\text{i}}}{e} + 0.35\left\langle V_{\text{i}\parallel}\right\rangle. \tag{7}$$

In H-mode standard discharges, the mean impurities parallel velocity, approximated by their toroidal velocity, is typically $< 10^4$ m/s at the plasma edge before the L-H transition. Since $\left\langle V_{\text{i}\parallel}\right\rangle$ is unavailable for deuterium ions, we assume that the mean main ion parallel velocity is equal to that of impurities. On the other hand, since the plasmas are all heated by NBI in the co-current direction, the edge $\left\langle V_{\text{i}\parallel}\right\rangle$ profile should not vary too much in our discharges. Thus, we can take $0.35\left\langle V_{\text{i}\parallel}\right\rangle$ as a constant ~ 3.5 kV/m before the L-H transition for all discharges in our dataset.

As the edge CXRS diagnostic was installed in 2009, the direct measurement of the E_r profiles using the CXRS is unavailable for our carbon PFCs dataset. However, $E_{r,\text{neo}}$ can be estimated from equation (7) using the routinely measured electron edge density and temperature profiles. According to [11, 21], the minimum of the radial electric field is always located just inside the separatrix, therefore $\rho_{\text{pol}} = 0.995$ is artificially chosen as the radial

position where the minimum of the radial electric field is expected. In the following, we describe how each term in equation (7) is estimated from the profile data in order to calculate $E_{r,\mathrm{neo}}$.

The inverse density gradient length $\nabla n_\mathrm{e}/n_\mathrm{e}$ can simply be calculated by dividing the density gradient values (applying the LAD method) in figure 3 by the corresponding edge density at $\rho_\mathrm{pol} = 0.995$. $P_\mathrm{L\text{-}H}$ versus the results taken in a time interval of 40 ms just before the L-H transition are plotted in figure 8. The values of $\nabla n_\mathrm{e}/n_\mathrm{e}$ in the carbon wall discharges are around -0.45 cm^{-1}, while they are around -0.57 cm^{-1} in the discharges with full tungsten PFCs. The absolute values of $\nabla n_\mathrm{e}/n_\mathrm{e}$ are on average larger in the full metal wall discharges compared to those with carbon PFCs.

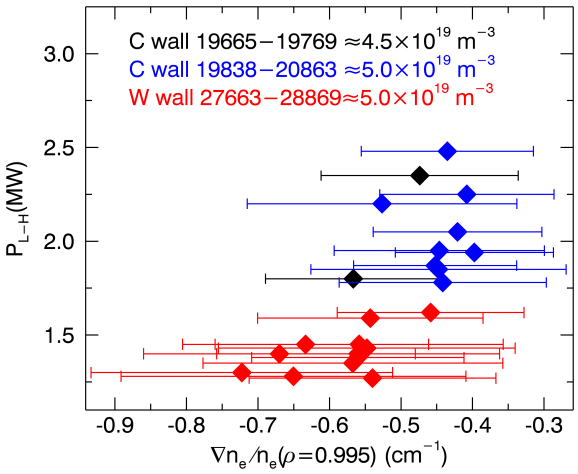

Figure 8: Power threshold versus inverse density gradient length $\nabla n_\mathrm{e}/n_\mathrm{e}$. The black and blue diamonds represent the discharges in C wall with core line-averaged densities of 4.5 and 5×10^{19} m^{-3}, respectively. Red diamonds indicate full W PFCs shots with a core line-averaged density of 5×10^{19} m^{-3}.

The electron temperatures for discharge #28869 with full metal PFCs before the L-H transition are 0.183 keV at $\rho_\mathrm{pol} = 0.98$ (the violet vertical dashed dotted line) and 0.116 keV at the separatrix (the black vertical solid line) shown as an example in figure 9(a). The ion temperatures seen in figure 9(b) provided by CXRS at the same positions are 0.182 keV and 0.144 keV. Here B^{5+} $(n = 7 \rightarrow 6)$ charge exchange line at 494.467 nm is used for the CXRS measurements. These differences between T_e and T_i at the plasma edge are confirmed by the analysis of the 7 discharges for which the edge ion temperature profiles are available. We find that the electron temperatures are higher inside of $\rho_\mathrm{pol} = 0.98$ and lower outside of $\rho_\mathrm{pol} = 0.98$, but similar to ion temperatures at $\rho_\mathrm{pol} = 0.98$ before the L-H transition. T_e and T_i at the pedestal top are close to each other for $n_\mathrm{e,ped} \geq 2 \times 10^{19}$ m^{-3} and heating powers in the range of $P_\mathrm{L\text{-}H}$ [25], but at the separatrix T_i is somewhat larger than T_e. Therefore, we assume $T_\mathrm{i} = T_\mathrm{e}$ at $\rho_\mathrm{pol} = 0.98$ and $T_\mathrm{i} = 0.14$ keV at the separatrix. The ion temperature profile is almost linear at the plasma edge, thus the edge ion temperature

gradients can simply be estimated as $\nabla T_\mathrm{i} = \frac{T_\mathrm{i}(0.98) - T_\mathrm{i}(1.00)}{r(0.98) - r(1.00)}$. Under the same assumption, the ion temperature at $\rho_\mathrm{pol} = 0.995$ (the blue vertical dashed lines in figure 9) can be estimated as $T_\mathrm{i}(0.995) = \frac{T_\mathrm{i}(0.98) + 3T_\mathrm{i}(1.00)}{4}$.

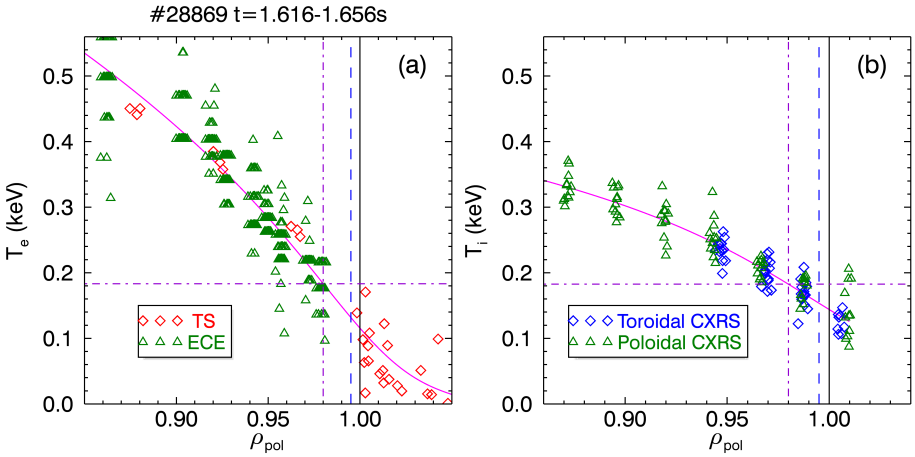

Figure 9: Edge electron (a) and ion (b) temperature profiles comparison for #28869. (a) The red diamonds are T_e profiles from combined core TS and edge TS, and the green triangles are T_e profiles from ECE. (b) The blue diamonds are ion temperatures from the toroidal edge CXRS and green triangles are T_i profiles from the poloidal edge CXRS. The dark violet vertical dashed dotted line, blue vertical dashed line and black vertical solid line are located at $\rho_\mathrm{pol} = 0.98, 0.995$ and the separatrix. The magenta curves are fits to electron and ion temperatures applying a MTanh function. The time slice is chosen from 1.616 to 1.656 s, i.e. from 40 ms before to the L-H transition.

The calculation of the factor α in equation (7) requires the ion collisionality $\nu_{*\mathrm{i}}$ [32] at $\rho_\mathrm{pol} = 0.995$. For our dataset, $\nu_{*\mathrm{i}}$ varies between 1.40 and 4.52 before the L-H transitions. Hence, the factor α in the plateau-collisional regime [14] is written as

$$\alpha = \frac{(\beta_1, g_{2\mathrm{i}}) - 2.1{\nu_{*\mathrm{i}}}^2\epsilon^3}{1 + {\nu_{*\mathrm{i}}}^2\epsilon^3}, \tag{8}$$

where ϵ is the inverse aspect ratio and $(\beta_1, g_{2\mathrm{i}}) = \frac{1.17 - 0.35{\nu_{*\mathrm{i}}}^{1/2}}{1 + 0.7{\nu_{*\mathrm{i}}}^{1/2}}$. According to equations (5) and (7) and the terms $\frac{\nabla n_\mathrm{e}}{n_\mathrm{e}}(0.995)$, $T_\mathrm{i}(0.995)$, ∇T_i and α calculated as just described, the minimum radial electric fields $E_{r,\mathrm{dia}}(0.995)$ and $E_{r,\mathrm{neo}} - \frac{B}{B_\mathrm{t}} B_\theta \left\langle V_{\mathrm{i}\parallel} \right\rangle (0.995)$ are estimated.

The minimum of the E_r well is plotted in figure 10 versus $\nabla n_\mathrm{e}/n_\mathrm{e}$ and $P_\mathrm{L\text{-}H}$. The black and blue symbols represent the discharges in carbon wall with core line-averaged densities of 4.5×10^{19} m^{-3} and 5×10^{19} m^{-3} corresponding to the collisionality dependent factor of $\alpha \in [0.208, 0.283]$ and $\alpha \in [-0.083, 0.040]$ at $\rho_\mathrm{pol} = 0.995$. The red ones stand for discharges with full tungsten PFCs with a core line-averaged density of 5×10^{19} m^{-3} and the collisionality dependent factor of $\alpha \in [-0.651, -0.292]$ at $\rho_\mathrm{pol} = 0.995$. The values of the minimum of $E_{r,\mathrm{neo}} - 0.35 \left\langle V_{\mathrm{i}\parallel} \right\rangle$ shown in figures 10(a) and (b) are constant around -13 kV/m within the errorbars in a wide range of the inverse density gradient length and threshold power with

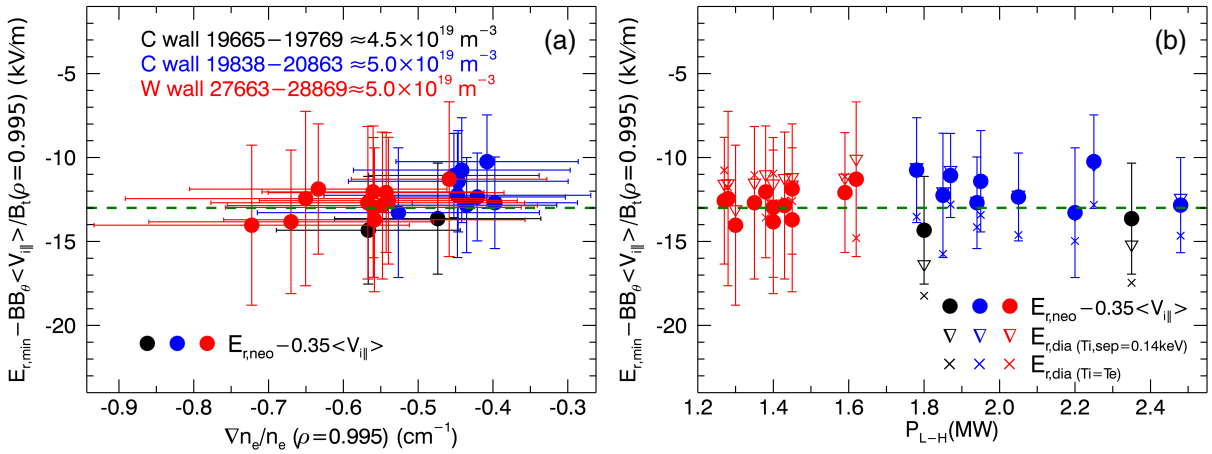

Figure 10: Radial electric fields at $\rho_{\rm pol} = 0.995$ versus (a) inverse density gradient length and (b) L-H transition power threshold evaluated according to equations (5) and (7). The filled circles (with errorbars) and the open triangles down (without errorbars in (b)) present $E_{r,\rm neo}$ and $E_{r,\rm dia}$ taking $T_{\rm i} = T_{\rm e}$ at $\rho_{\rm pol} = 0.98$ and $T_{\rm i} = 0.14$ keV at the separatrix. The crosses correspond to calculated $E_{r,\rm dia}$ taking $T_{\rm i} = T_{\rm e}$ at the plasma edge.

similar core line-averaged densities. This value is well consistent with $E_{r,\rm neo} \approx -15$ kV/m found for a wide range of pedestal top densities as described in reference [25]. As analyzed before, $0.35\left\langle V_{\rm i\|}\right\rangle(0.995)$ could be almost the same for all discharges. These results suggest that the minimum edge $E_{r,\rm neo}$, just before the L-H transition, is a constant value in different PFCs despite different inverse density gradient length as well as threshold power. We also compare the evaluated $E_{r,\rm dia}(0.995)$ taking $T_{\rm i} = 0.14$ keV at the separatrix ($T_{\rm i} = T_{\rm e}$ at $\rho_{\rm pol} = 0.98$) and $T_{\rm i} = T_{\rm e}$ at the plasma edge as shown in figure 10(b). It shows that when choosing $T_{\rm i} = 0.14$ keV at the separatrix, the calculated $E_{r,\rm dia}(0.995)$ are much closer in the discharges with both PFCs. The L-H transition with the full tungsten wall occurs at a lower heating power and therefore flatter temperature gradient compensated by a steeper density gradient, leading to the same $E_{r,\rm neo}$ well as in carbon wall.

5. Discussion and conclusions

The power threshold $P_{\rm L\text{-}H}$ is lower in full tungsten wall discharges than in carbon wall by 25% at ASDEX Upgrade [4]. It is assumed that the radial electric field shear $\frac{\partial E_r}{\partial r}$ is the critical parameter for access to the H-mode [42]. We have analyzed the edge profiles and other quantities which could effect $\frac{\partial E_r}{\partial r}$ are discussed below. The radiated power $P_{\rm rad}$ is found to be similar before the L-H transition in both carbon and full tungsten wall discharges. Therefore, a tiny change of the radiated power due to the different impurity composition is not the cause for the lower $P_{\rm L\text{-}H}$ in the full tungsten wall discharges. In the full tungsten wall discharges, a sharp impurity concentration decrease happens after boronization in ASDEX Upgrade [3]. However, in the 2008 campign $P_{\rm L\text{-}H}$ was reduced by $\sim$ 25% without boronization [4], in

which the impurity concentration is close to that in the carbon walls. Thus, the suppression of the main ion dilution seems not to be the cause of the decreased $P_{\text{L-H}}$ in the full tungsten wall discharges. Power threshold studies with low plasma density in the DIII-D tokamak using NBI torque variation with counter-current and co-current beams [43] and in ASDEX Upgrade applying NBI power scans at fixed electron cyclotron resonant heating power P_{ECRH} [44], reveal that $P_{\text{L-H}}$ increases with the rise of the parallel edge plasma rotation $\left\langle V_{\text{i}\parallel} \right\rangle$. This can be explained as that the higher parallel rotation contributing to higher $\frac{B}{B_{\text{t}}} B_\theta \left\langle V_{\text{i}\parallel} \right\rangle$ relaxes the negative edge radial electric field [15], which is a key parameter for the L-H transition. However, for high density deuterium plasmas, no difference between ECRH heating or NBI heating only is found within the error bars as shown in figure 4 of reference [45]. Therefore, in our dataset, we do not take the effect of the parallel rotation term $\frac{B}{B_{\text{t}}} B_\theta \left\langle V_{\text{i}\parallel} \right\rangle$ on the evaluated $E_{r,\text{neo}}$ into account, since the parallel velocity is small and should not vary too much for our discharges. Further studies show that neither the magnetic shape nor gas fuelling position (from main chamber or divertor) has an impact on $P_{\text{L-H}}$ on ASDEX Upgrade. Therefore, in ASDEX Upgrade, we conclude that the lower $P_{\text{L-H}}$ is caused by steeper edge density gradients in the full tungsten wall discharges.

The higher gas fuelling (maybe assisted by the higher reflection coefficient) in full tungsten wall discharges leads to the fluctuating detachment state and complete detachment state in the divertor. A longer phase of fluctuating and complete divertor detachment (> 550 ms) is found in full tungsten wall discharges, while it is much shorter (~ 40 ms) and disappears far before the L-H transition in the carbon PFCs. As confirmed by comparing edge density profiles in the same and different PFCs discharges, the edge density profile is steeper and the edge density top is higher as soon as the divertor reaches the fluctuating detachment state. This is thought to be the main reason for the steeper edge density gradient. The higher recycling coefficient of full tungsten wall compared to carbon wall also plays a role for steeper edge density profile. However, the impact of decreased impurity concentration on particle transport is still unclear, and it will be the subject of future investigations.

In summary, when the plasma facing material was fully replaced by tungsten, a lower power threshold and a steeper edge density gradient were achieved before the L-H transition. As main difference, the steeper edge density gradients in full tungsten wall plasmas are identified leading to steeper edge pressure gradients and, through neoclassic theory, leading to a deeper E_r well at otherwise identical plasma conditions. Taking into account the measured edge kinetic profiles, the calculated minimum $E_{r,\text{neo}}$ is found to be the same for both wall materials before the L-H transition. This shows that not only the ion heat flux at the plasma edge [44] but also the edge electron density gradient plays a role for $P_{\text{L-H}}$.

Acknowledgments

This work has been carried out within the framework of the EUROfusion Consortium and has received funding from the Euratom research and training programme 2014-2018 under grant agreement No 633053. The views and opinions expressed herein do not necessarily

reflect those of the European Commission. L. M. Shao is a fellow of the jointly financed CAS-MPG Doctoral Promotion Programme and F. M. Laggner is a fellow of the Friedrich Schiedel Foundation for Energy Technology.

References

[1] Martin Y R, *et al.* 2008 *J. Phys. Conf. Ser.* **123** 012033.
[2] Neu R, *et al.* 2007 *J. Nucl. Mat.* **367** 1497-502.
[3] Neu R, *et al.* 2013 *J. Nucl. Mat.* **438** S34-S41.
[4] Ryter F, *et al.* 2013 *Nucl. Fusion* **53** 113003.
[5] Maggi C F, *et al.* 2014 *Nucl. Fusion* **54** 023007.
[6] Bourdelle C, *et al.* 2014 *Nucl. Fusion* **54** 022001.
[7] Gohil P, Evans T E, Fenstermacher M E, Ferron J R, Osborne T H, Park J M, Schmitz O, Scoville J T and Unterberg E A 2011 *Nucl. Fusion* **51** 103020.
[8] Ma Y, Hughes J W, Hubbard A E, LaBombard B and Terry J 2012 *Plasma Phys. Control. Fusion* **54** 082002.
[9] Valović M, Garzotti L, Gurl C, Akers R, Harrison J, Michael C, Naylor G, Scannell R and the MAST team 2012 *Nucl. Fusion* **52** 114022.
[10] Cui Z Y *et al.* 2014 *41st EPS Conference on Plasma Physics* P4.003.
[11] Conway G D, Angioni C, Ryter F, Sauter P and Vicente J 2011 *Phys. Rev. Lett.* **106** 065001.
[12] Schmitz L, Zeng L, Rhodes T L, Hillesheim J C, Doyle E J, Groebner R J, Peebles W A, Burrell K H and Wang G 2012 *Phys. Rev. Lett.* **108** 155002.
[13] Xu M *et al.* 2012 *Phys. Rev. Lett.* **108** 245001.
[14] Hinton F and Hazeltine R 1976 *Rev. Mod. Phys.* **48** 239-308.
[15] Stroth U, Manz P and Ramisch M 2011 *Plasma Phys. Control. Fusion* **53** 024006.
[16] Biglari H, Diamond P H and Terry P W 1990 *Phys. Fluids B* **2** 1.
[17] Burrell K H 1997 *Phys. Plasmas* **4** 1499-518.
[18] Wagner F 2007 *Plasma Phys. Control. Fusion* **49** B1-B33.
[19] Pütterich T, Wolfrum E, Dux R and Maggi C 2009 *Phys. Rev. Lett.* **102** 025001.
[20] Viezzer E, Pütterich T, Dux R and McDermott R M 2012 *Rev. Sci. Instrum.* **83** 103501.
[21] Viezzer E, *et al.* 2013 *Nucl. Fusion* **53** 053005.
[22] Viezzer E, Pütterich T, Angioni C, Bergmann A, Dux R, Fable E, McDermott R M, Stroth U and Wolfrum E 2014 *Nucl. Fusion* **54** 012003.
[23] Marr K D, Lipschultz B, Catto P J, McDermott R M, Reinke M L and Simakov A N 2010 *Plasma Phys. Control. Fusion* **52** 055010.
[24] Kagan G, Marr K D, Catto P J, Landreman M, Lipschultz B and McDermott R 2011 *Plasma Phys. Control. Fusion* **53** 025008.
[25] Sauter P, Pütterich T, Ryter F, Viezzer E, Wolfrum E, Conway G D, Fischer R, Kurzan B, McDermott R M and Rathgeber S K 2012 *Nucl. Fusion* **52** 012001.
[26] Ryter F, Fahrbach H-U, Gude A, Neu R, Rohde V, Stober J and the ASDEX Upgrade Team 2002 *Plasma Phys. Control. Fusion* **44** A407-13.
[27] Fischer R, Wolfrum E and Schweinzer J 2008 *Plasma Phys. Control. Fusion* **50** 085009.
[28] Rathgeber S K, Barrera L, Eich T, Fischer R, Nold B, Suttrop W, Willensdorfer M and Wolfrum E 2013 *Plasma Phys. Control. Fusion* **55** 025004.
[29] Kurzan B and Murmann H D 2011 *Rev. Sci. Instrum.* **82** 103501.
[30] Mlynek A, Schramm G, Eixenberger H, Sips G, McCormick K, Zilker M, Behler K, Eheberg J and ASDEX Upgrade Team 2010 *Rev. Sci. Instrum.* **81** 033507.
[31] Bernert M, Eich T, Burckhart A, Fuchs J C, Giannone L, Kallenbach A, McDermott R M, Sieglin B and the ASDEX Upgrade Team 2014 *Rev. Sci. Instrum.* **85** 033503.

[32] Sauter O, Angioni C and Liu-Liu Y R 1999 *Phys. Plasmas* **6** 2834.
[33] Groebner R J, Baker D R, Burrell K H, Carlstrom T N, Ferron J R, Gohil P, Lao L L, Osborne T H, Thomas D M and West W P 2011 *Nucl. Fusion* **41** 1789.
[34] Eakambaram S and Elangovan R 2011 *Least Absolute Deviation Regression Theory and Methods* LAP LAMBERT Academic Publishing p 120.
[35] Potzel S, Wischmeier M, Bernert M, Dux R, Müller H W and Scarabosio A 2014 *Nucl. Fusion* **54** 013001.
[36] Kallenbach A, *et al.* 2010 *Plasma Phys. Control. Fusion* **52** 055002.
[37] Wischmeier M, *et al.* 2009 *J. Nucl. Mat.* **390-391** 250-254.
[38] Surface Interaction Database. *EIRENE* www.eirene.de/html/deuterium.html.
[39] Feng Y, Sardei F, Kisslinger J, Grigull P, McCormick K and Reiter D 2004 *Contrib. Plasma Phys.* **44** 57-69.
[40] Lunt T, Carralero D, Feng Y, Birkenmeier G, Müller H W, Müller S, Wischmeier M, the ASDEX Upgrade team 2015 *J. Nucl. Mat.* **463** 744-747.
[41] Schneider W, McCarthy P J, Lackner K, Gruber O, Behler K, Martin P and Merkel R 2000 *Fusion Eng. Des.* **48** 127-34.
[42] Burrell K H, *et al.* 1992 *Plasma Phys. Control. Fusion* **34** 1859.
[43] Gohil P, Jernigan T C, Osborne T H, Scoville J T and Strait E J 2010 *Nucl. Fusion* **50** 064011.
[44] Ryter F, Barrera Orte L, Kurzan B, McDermott R M, Tradini G, Viezzer E, Bernert M and Fischer R 2014 *Nucl. Fusion* **54** 083003.
[45] Ryter F, *et al.* 2009 *Nucl. Fusion* **49** 062003.